STUDIA UBB CHEMIA, LVI, 4, 2011 (p. 49 - 54)

A COMPUTATIONAL INVESTIGATION OF THE DECAY MECHANISM OF THE REACTION PRODUCT OF ANTHRANILATE DIOXYGENASE (ANTHRANILIC ACID DIOL)

RADU SILAGHI-DUMITRESCU[a,*], RADU GHINGA[b]

ABSTRACT. Anthranilate diol is a non-aromatic dihydrodiol produced during the enzymatic degradation of anthranilate by anthranilate dioxygenase. The anthranilate diol is generally accepted to decompose spontaneously to catechol, thus regaining aromaticity. The present study employs density functional (DFT), Hartree-Fock (HF) and AM1 calculations to examine the mechanism of anthranilate diol decomposition.

Keywords: *anthranilate, anthranilate diol, Rieske dioxygenase, catechol, DFT*

INTRODUCTION

Rieske dioxygenases (RDO) are non-heme iron enzymes catalyzing the cis-1,2 di-hydroxylation of aromatic substrates, producing non-aromatic dihydrodiols. Within this family of enzymes, anthranilate dioxygenase catalyzes the transformation of anthranilate (2-aminobenzoate) to the corresponding diol, which then further decomposes to catechol and regains its aromaticity as shown in *Figure* 1.

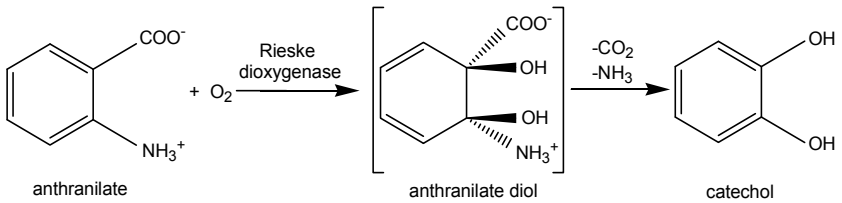

Figure 1. The reaction catalyzed by anthranilate dioxygenase, followed by decomposition of the diol.

[a] Universitatea Babeş-Bolyai, Facultatea de Chimie şi Inginerie Chimică, Str. Kogălniceanu, Nr. 1, RO-400084 Cluj-Napoca, Romania, * *rsilaghi@chem.ubbcluj.ro*
[b] Grup Şcolar de Transporturi Auto "Henri Coandă", Str. Mărăşeşti, Nr. 34, RO-310332 Arad, Romania, radughinga@gmail.com

One currently assumes that this latter decomposition occurs spontaneously; it is, however, not known precisely whether this requires assistance from the enzyme or if it occurs after liberation of the diol from the active site. The atomic-level details of this process are, likewise, not known. The present paper reports a computational investigation aiming to evaluate the stability and decomposition pathway of the anthranilate diol.

RESULTS AND DISCUTIONS

Equilibrium geometries

Figure 2 shows optimized geometries for the anthranilic acid diol - neutral and zwitterions, and Table 1 shows key bond lengths and distances in anthranilate and anthranilate diol, as computed with HF/6-31G**, BP86/6-31G**, and AM1.

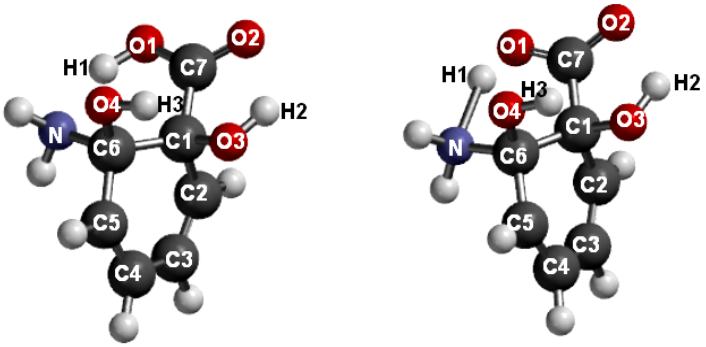

Figure 2. BP86-optimized geometry for the anthranilate diol – neutral vs. zwitterion.

For the diol, the BP86 and the HF methods (but not AM1) failed to locate a minimum on the potential energy surface; instead, upon geometry optimization one of the NH_3 protons migrated to the nearby carboxylate oxygen. However, for the anthranilic acid even the AM1 failed in producing a zwitterionic geometry. Table 1 shows that the C-C bonds within the phenyl ring in anthranilic acid range within 0.03-0.04 Å of each other as expected for an aromatic compound, whereas again as expected in the corresponding diol (based on AM1 results) the C-C bonds range from 1.34 Å (typical for a double bond) to 1.57 Å for the C1-C6 bond involving the substituted carbon atoms (slightly longer than a typical single bond).

Table 1. Key bond lengths and distances in the anthranilate diol and anthranilic acid (in Å), as computed with HF/6-31G**, BP86/6-31G**, and AM1 (cf. Figure 1).

	Anthranilate diol				Anthranilate		
	Neutral			Zwitterion	Neutral		
bond	BP86	HF	AM1	AM1	BP86	HF	AM1
C6-N	1.51	1.47	1.46	1.54	1.37	1.37	1.38
C6-O4	1.41	1.39	1.44	1.41	-	-	-
C1-O3	1.44	1.40	1.42	1.42	-	-	-
C1 -C7	1.57	1.55	1.53	1.59	1.49	1.49	1.47
C1-C2	1.52	1.52	1.50	1.50	1.42	1.40	1.40
C2-C3	1.35	1.32	1.34	1.34	1.39	1.37	1.39
C3-C4	1.47	1.48	1.45	1.45	1.41	1.39	1.40
C4-C5	1.35	1.32	1.34	1.34	1.39	1.37	1.38
C5-C6	1.52	1.52	1.52	1.51	1.42	1.40	1.43
C1-C6	1.57	1.55	1.59	1.57	1.44	1.41	1.42
C7-O1	1.32	1.30	1.36	1.26	1.37	1.33	1.39
C7-O2	1.23	1.19	1.23	1.25	1.23	1.19	1.24
N-H1	1.56	1.80	2.69	1.04	4.56	4.46	4.44
O1-H1	1.05	0.96	0.97	2.01	0.98	0.94	0.97
O3---H3	1.94	2.13	2.24	2.04	-	-	-
O2---H2	1.86	2.01	2.27	2.01	-	-	-
O4-H3	0.99	0.95	0.97	0.97	-	-	-
O3-H2	1.00	0.95	0.97	0.98	-	-	-

Decomposition pathways

Figure 3 shows the decomposition pathways computed for the anthranilic acid diol, with HF/6-31G** and BP86/6-31G** following the C---N coordinate (i.e., cleavage of the C-NH2 bond). Figure 4 shows the decomposition pathways following the C---CO2 coordinate.

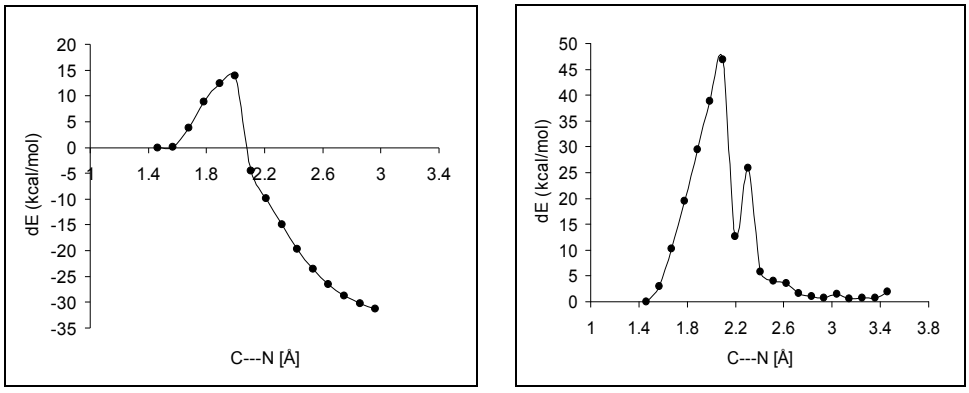

Figure 3. DFT and HF energy profiles assuming a reaction coordinate where the C---N distance is elongated. Relative energies are given.

The ~30 kcal/mol difference seen in Figure 3 in apparent activation energies computed with HF and DFT following the C---N coordinate can be explained by the fact that in the DFT calculations a proton transfer occurs early on the potential energy surface, transforming the NH_2 substituent into NH_3, which then facilitates liberation of ammonia almost concerted with liberation of CO_2.

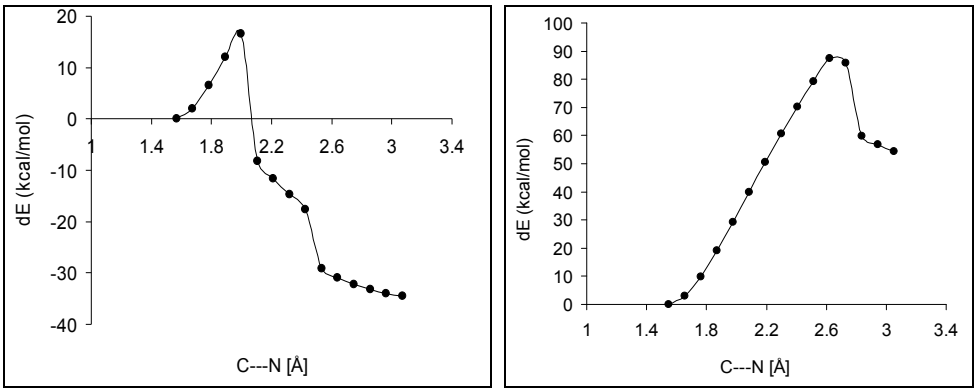

Figure 4. DFT and HF energy profiles assuming a reaction coordinate where the C---CO2 distance is elongated. Relative energies are given.

By contrast, in the HF-computed potential energy surface the CO_2 remains bonded to the molecule. A similar result is obtained in Figure 4, where the apparent activation energies computed by the two methods differ by ~70 kcal/mol; here, following the C---CO_2 coordinate the NH_3 remains bonded to the benzene ring with HF throughout the calculations, whereas it spontaneously dissociates from the benzene ring, almost concerted with dissociation of CO_2, in the DFT calculations. Thus, DFT appears to have located, in both cases, lower-energy pathways than HF. Importantly, these lower-energy pathways involve concerted breaking of two bonds as opposed to one. This fact, together with the asymetry in the DFT-derived potential energy curves in Figures 3 and 4 (with much steeper slopes to the right of the transition state), as well as the fact that HF predicts prohibitevly high energy barriers, all suggest the need for examining the reaction barrier along more than one coordinate. Therefore, Figure 5 shows potential energy surfaces where the two reaction coordinates are monitored concomitantly. It may be seen that the lowest-energy pathway connecting the reactant with the product does involve elongation along both coordinates, with the C-N bond elongated more than the C-C bond (at the saddle point, the C-C bond is 1,77 Å and the C-N bond is 1,94 Å with DFT and, for HF, the C-C bond is 1,86 Å and the C-N bond is 1,99 Å).

Figure 6 shows a two-dimensional representation of the lowest-energy pathways from Figure 5, illustrating how the asymmetry initially noted for the single-coordinate curves of Figures 3 and 4 has now disappeared, and showing

how the computed activation energies are now reasonable with DFT as well as with HF. Nevertheless, it is particularly important to note that the values predicted by the two methods differ by ~25 kcal/mol, which, considering that one of the values is 15 kcal/mol, represents a very large difference. Indeed, based on the DFT data the anthranilic acid diol should be disappearing within a millisecond timescale, whereas the HF data suggests that the diol should be detectable on a longer time-scale.

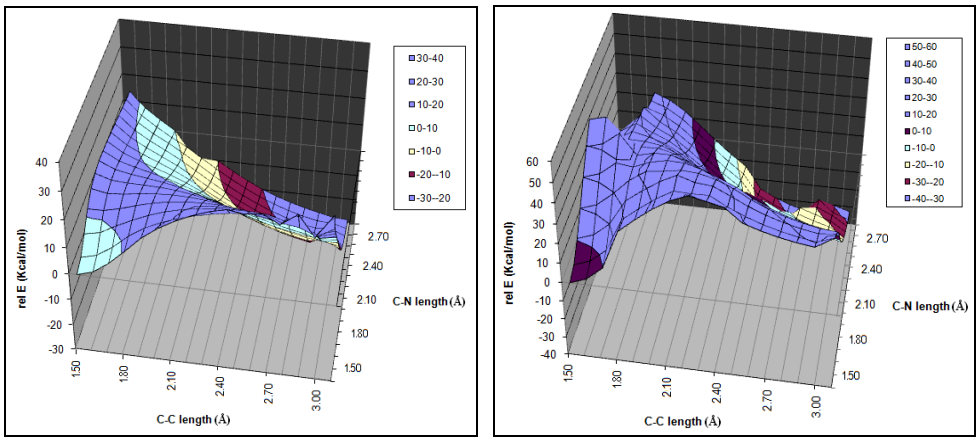

Figure 5. 3-D charts for the anthranilate diol decomposition as computed with BP86/6-31G** and HF/6-31G**following C---N and C---CO_2 coordinates simultaneously.

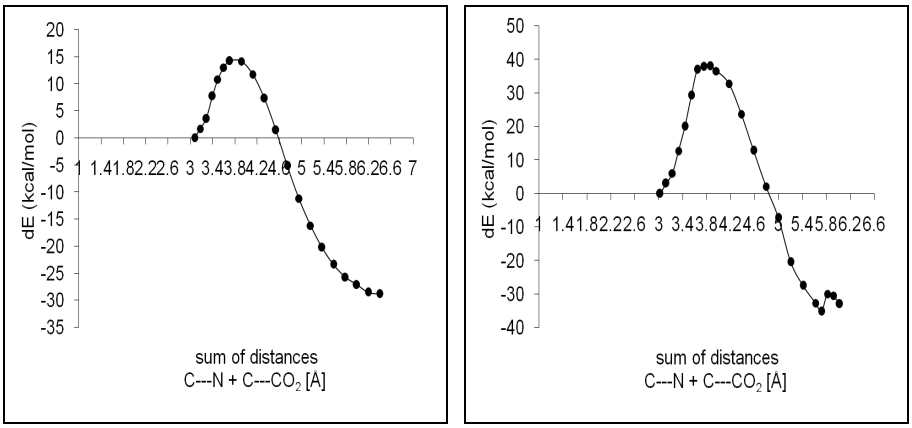

Figure 6. Section of the 3-D chart (see fig.6) for the anthranilate diol decomposition as computed with BP86/6-31G** and HF/6-31G** following C---N and C---CO2 coordinates simultaneously (data extracted from Figure 5).

To conclude, the decomposition pathway for decomposition of the anthranilic acid diol has been identified in detail, and shown to involve quasi-simultaneous elongation of the carbon-ammonia and carbon-CO_2 bond lengths. On the methodological side, a failure of the computational methods in yielding optimized geometries for the amfionic structures is noted, as is the unacceptably large difference in activation energies computed by DFT vs HF – a difference which has qualitative and not only quantitative consequences on the predictions made by the two methods.

METHODS

The present study employs three calculation methods: the BP86 density functional method using the 6-31G** basis set, Hartree-Fock with the 6-31G** basis set, and the semi-empirical method AM1, as implemented in the Spartan software package.[12]

ACKNOWLEDGEMENT

Financial support from the Romanian Ministry for Education and Research, grant PCCE-140/2008, is gratefully acknowledged.

REFERENCES

1. L.P. Wackett, *Enzyme and Microbial Technology*, **2002**, *31*, 577.
2. B.M. Bundy, A.L. Campbell, E.L. Neidle, *J Bacteriology,* **1998**, *180*(17), 4466.
3. A. Ichihara, K. Adachi, K. Hosokawa, Y. Takeda, *The Journal Of Biological Chemistry,* **1962**, *237*, 2296.
4. R. Silaghi-Dumitrescu, *Studia UBB Chemia*, **2007**, *2*, 103.
5. H.K. Chang, P. Mohseni, G.J. Zylstra, *J Bacteriology,* **2003**, *185*(19), 5871.
6. P.D. Oldenburg, Y Feng, I. Pryjomska-Ray, *Journal of The American Chemical Society*, *132*, 17713.
7. D.M. Kurtz, Z.M. Beharry, D.M. Eby et al., *Journal Of Inorganic Biochemistry,* **2001**, *86*, 304.
8. L.P. Wackett, *Enzyme and Microbial Technology,* **2002**, *31*, 577.
9. D.M. Eby, Z.M. Beharry, E.D. Coulter, *Journal of Bacteriology,* **2001**, *183*, 109.
10. P.D. Oldenburg, C.Y. Ke, L. Que, *Abstracts of Papers of the American Chemical Society*, **2007**, *233*, 173.
11. Z.M. Beharry, D.M. Eby, E.D. Coulter, R. Viswanathan, E.L. Neidle, R.S. Phillips, D.M. Kurtz Jr., *Biochemistry,* **2003**, 2542(46), 13625.
12. Spartan 5.0, Wavefunction, Inc., 18401 Von Karman Avenue Suite 370, Irvine, CA 92612 U.S.A.